Supplementary Material

Tendon-inspired robust ionic conductive hydrogels with multi-hierarchical structures towards asthmatic patients medication monitoring

Qi Zhou[a], Shengxu Lu[a], Pengwu Xu[a], Deyu Niu[a], Debora Puglia[b], Weijun Yang[a]*, Piming Ma[a]*

[a,] The Key Laboratory of Synthetic and Biological Colloids, Ministry of Education, School of Chemical and Material Engineering, Jiangnan University, Wuxi, 214122, China.

[b,] Civil and Environmental Engineering Department, Materials Engineering Center, Perugia University, UdR INSTM, Terni 05100, Italy.

Corresponding authors: weijun.yang@jiangnan.edu.cn; p.ma@jiangnan.edu.cn.

Table of contents:

S1 Characterization

Tensile tests were conducted at a rate of 10 mm/min, and compression tests were performed at a rate of 5 mm/min by using the universal testing machine (Instron, 5967X) at room temperature to assess the mechanical properties and fatigue resistance of the hydrogels. In the successive tensile loading-unloading experiments, the hydrogels were subjected to different strains (ranging from 0 to 500% for tensile tests) without intervals between cycles, and a fixed strain (300%) with recovery times (5 min, 10 min, 15 min, and 30 min, respectively). Additionally, in the cyclic compression experiment, the hydrogels were subjected to 100 cycles at 50% strain.

The electrochemical impedance spectroscopy (EIS) of the hydrogels was conducted using the electrochemical workstation (CHI 760E, Shanghai Chenhua Instrument) within a frequency range from 10^{-2} to 10^{6} Hz and a voltage of 0.1 V at room temperature. The ionic conductivity of the hydrogels was determined by the following formula: $\sigma=L/SR$, where σ (S/m) represents the ion conductivity, S (m^2) represents the cross-sectional area of the hydrogel, L (m) represents the thickness of the hydrogel, and R (Ω) signifies the intercept on the real axis (Z') of the Nyquist plot in the EIS experiment, respectively.

The water content (WC) and density (DS) of the hydrogels were determined using the following formulas: $WC = (M_1 - M_2) / M_1$, $DS = M_2 / V$, respectively. Where M_1 represents the initial weight of the hydrogel before drying, M_2 represents the weight of the hydrogel after drying, and V represents the volume of the hydrogel before drying, respectively. The morphology of the freeze-dried hydrogels was analyzed using field-emission scanning electron microscopy (SEM) (S4800, Hitachi) at an accelerating voltage of 5 kV. The rheological characterization of the hydrogels was performed at room temperature using a rotational rheometer (MCR302e, Anton Paar) with a strain of 1% and a frequency range of 0.1-100 rad/s. The FT-IR spectra was acquired using ATR/FT-IR (Nicolet iS50, Thermo Fisher) with a scanning range of 600-4000 cm^{-1}, a resolution of 4 cm^{-1} and 32 scans. The Raman spectra was recorded using a microscopic confocal Raman spectrometer (Renishaw, InVia) with an excitation wavelength of 532 nm and a scanning range of 4000-400 cm^{-1}. The freezing point of the hydrogels was

determined by differential scanning calorimetry (DSC) (DSC3, Mettler Toledo). The X-ray diffraction (XRD) pattern was obtained using an X-ray diffractometer (D8, Bruker AXS) with Cu-K_α radiation (λ = 1.5406 Å, 40 kV, 20 mA) with a scanning range of 5-50° and a scanning rate of 4 °/min. The high-resolution X-ray photoelectron spectroscopy (XPS) spectra of the freeze-dried hydrogels was acquired using an XPS instrument (AXIS Supra, Kratos) with AlK_α radiation, and all spectra were calibrated by C1s (284.8 eV).

S2 Sensing measurements

The relative resistance change (ΔR) of the hydrogels was measured at various strains (0.5%, 1%, 2%, 5%, 10%, 25%, 50%, 100%, and 200%) using both the electrochemical workstation and the universal mechanical testing machine. The sensitivity gauge factor (GF) of the hydrogels was calculated by the following formula: $GF = \Delta R/\varepsilon$, where ε represents the applied strain. Additionally, the hydrogels were subjected to over 1000 cycles of compression at 25% and 50% strain to assess signal stability during practical usage.

S3 Supplementary Figures

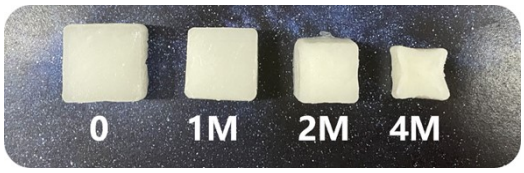

Fig. S1. Macroscopic photograph of the hydrogels.

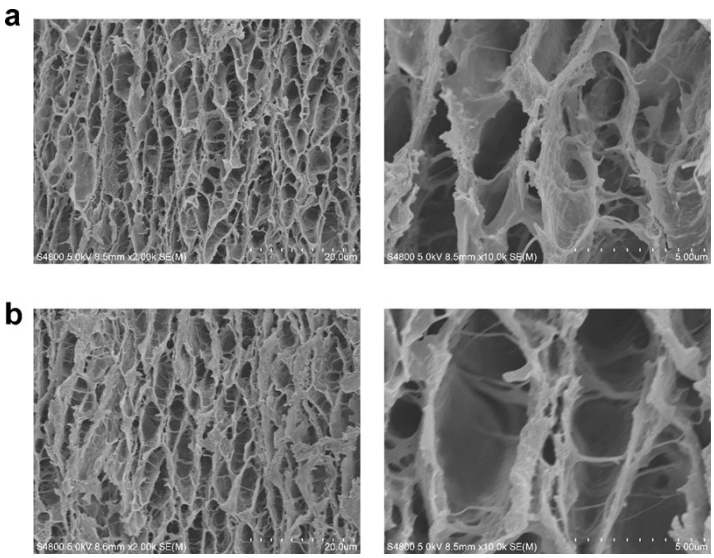

Fig. S2. Microscopic morphology of the PVA/CMC/CCNF-2M hydrogel before (a) and after (b) compression.

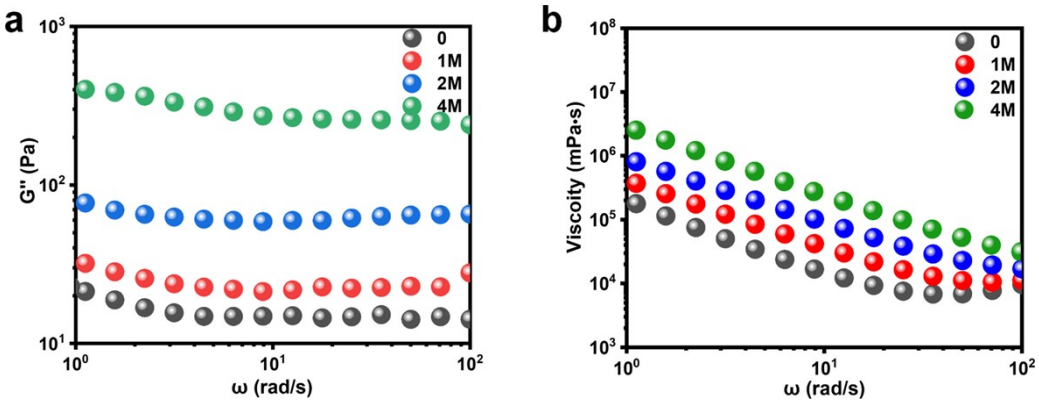

Fig. S3. Loss modulus and complex viscosity.

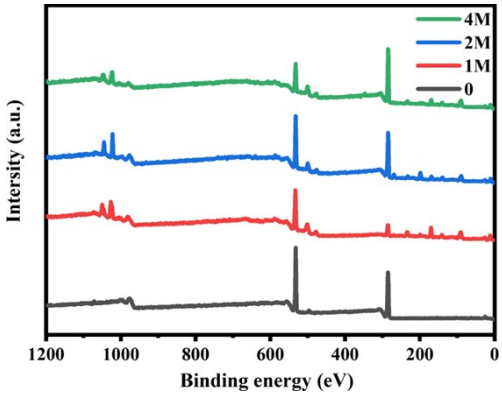

Fig. S4. X-ray photoelectron spectroscopy spectra.

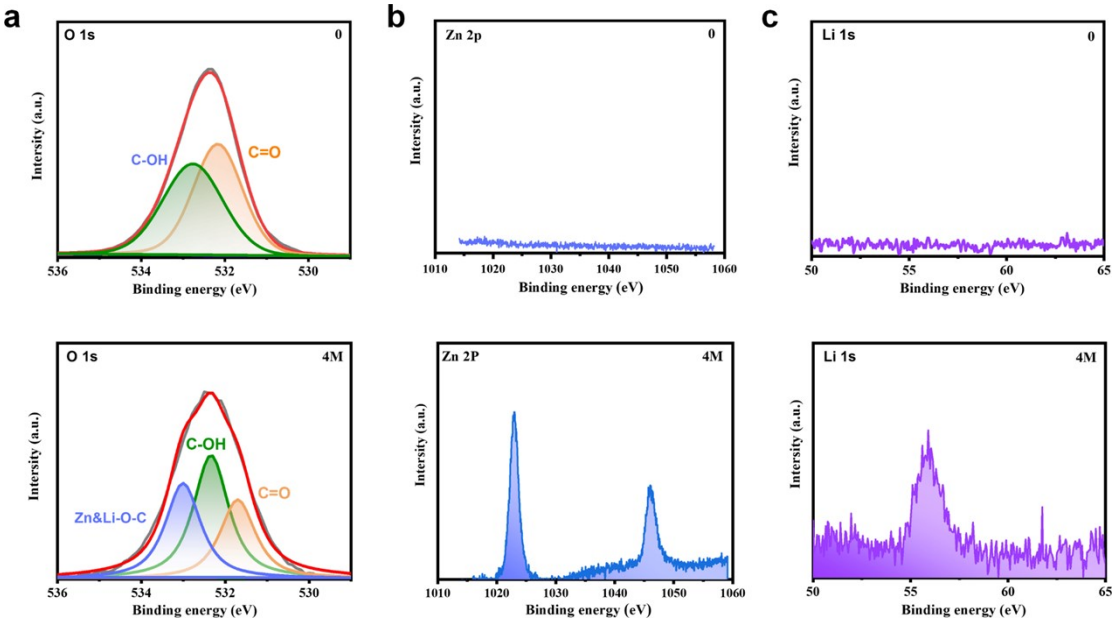

Fig. S5. X-ray photoelectron spectroscopy (XPS) spectra of O 1s, Li 1s, and Zn 2p for the PVA/CMC/CCNF hydrogel and the PVA/CMC/CCNF-4M hydrogel.

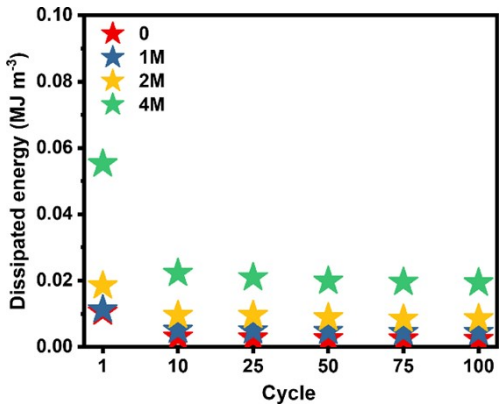

Fig. S6. Dissipative energy under different compression cycles.

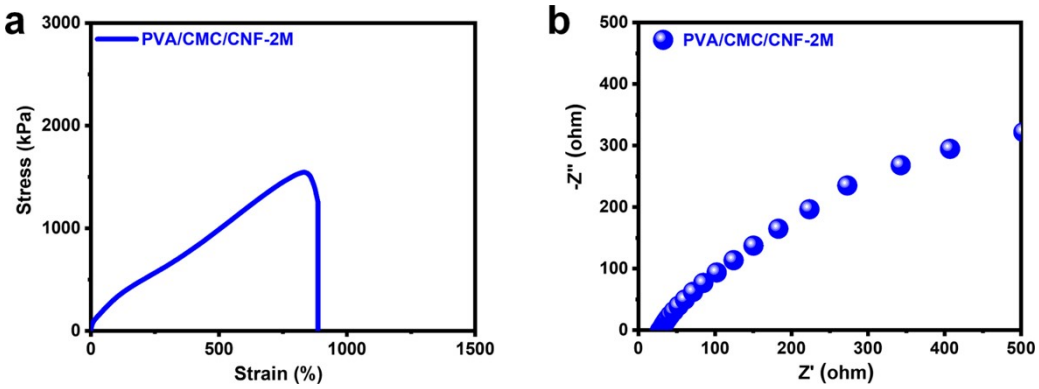

Fig. S7. The stress-strain curve and EIS spectra of the PVA/CMC/CNF-2M hydrogel at -5°C.

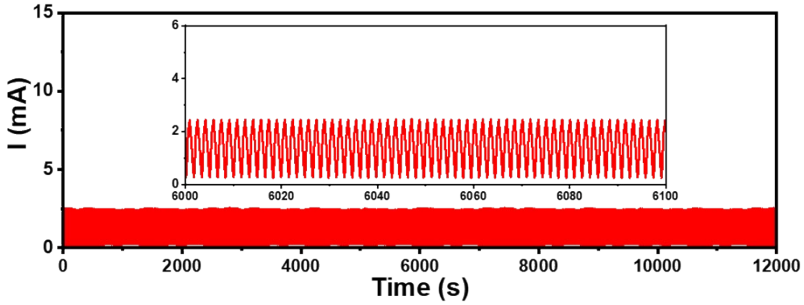

Fig. S8. The sensing stability over 5000 cycles.

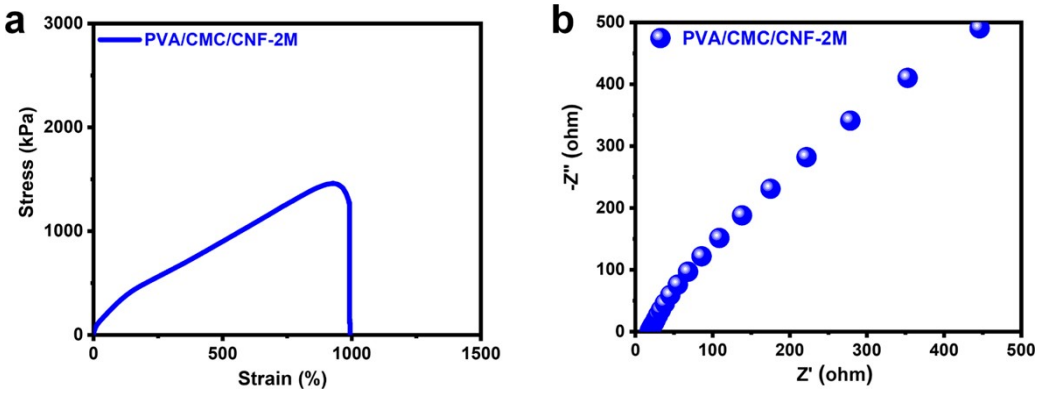

Fig. S9. The stress-strain curve and EIS spectra of the PVA/CMC/CNF-2M hydrogel after three months of storage.

S4 Potential applications in flexible zinc-ion batteries.

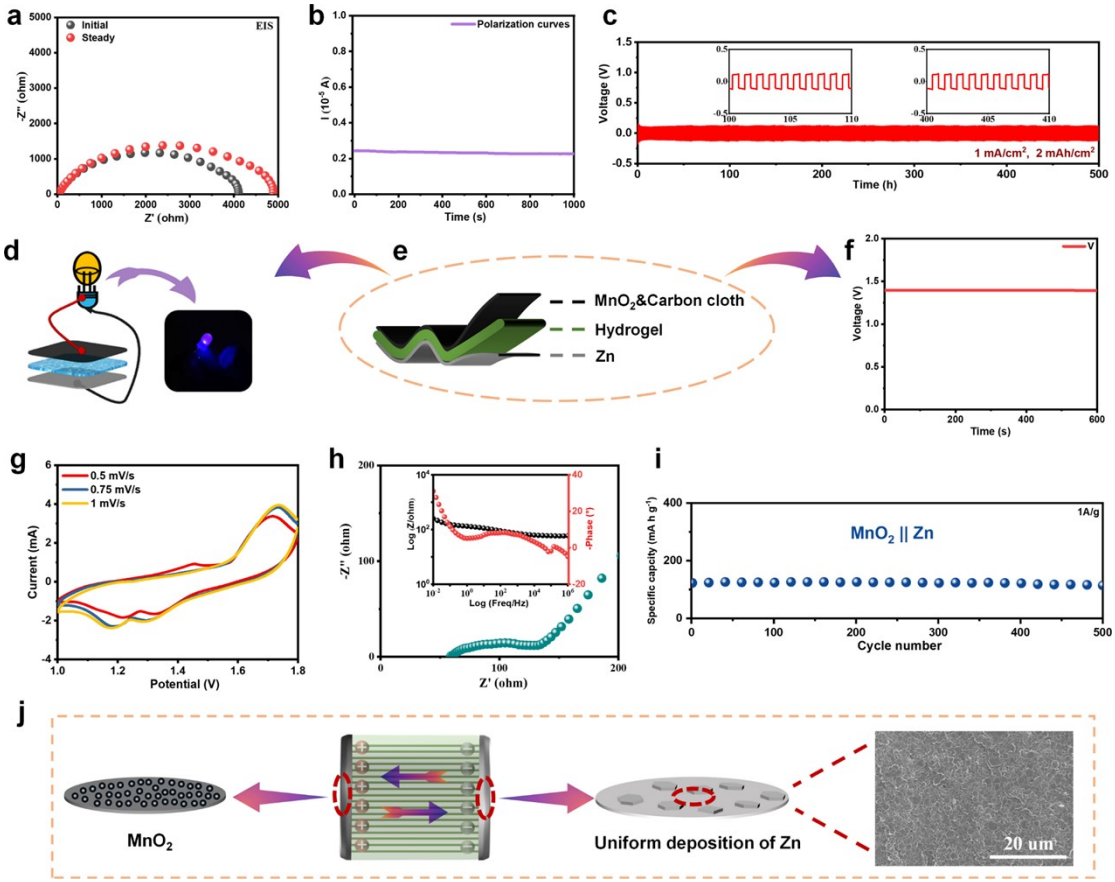

Fig. S10. (a) EIS spectra and (b) polarization curves before and after polarization. (c) Cycling performance over 500 cycles of zinc plating-stripping tests. (d) Photographs of the soft package battery powering an LED bulb. (e) The design principle of the MnO_2 || Zn soft package battery. (f) Voltage stability curves. (g) Cyclic voltammetry curves. (h) EIS spectra. (i) Cycling stability over 500 cycles. (j) The working principle of the battery and the suppression of the zinc dendrite growth.

Flexible zinc ion batteries are highly competitive miniature power sources, suitable as safe energy storage devices for flexible electronics.[1, 2] However, a major limitation to their lifespan is the growth of zinc dendrites.[3] Recent advanced studies have indicated that the mechanical strength of the battery separator significantly impacts the formation of Zn dendrites.[4] Specifically, when zinc dendrites encounter a high-strength separator, their upward growth is restricted, leading to a flat anode surface and preventing short-circuits caused by dendrite growth.[5]

Here, the PVA/CMC/CCNF-4M hydrogel with its excellent mechanical properties and compressive strength was utilized as an electrolyte to evaluate its ion transference number and cycling stability as a battery separator. From the EIS spectra and

polarization current curves before and after polarization, the ion transference number was determined to be 0.92, comparable to most hydrogel electrolytes (Fig. S9a and Fig. S9b).[6] This is attributed to the formation of ordered ionic channels and the rapid coordination and decoordination of metal ions with carboxyl groups on the polysaccharide chains, contributing to a significant ion transference number[7]. Additionally, as shown in Fig. S9c, the hydrogel maintains excellent cycling stability over 500 cycles at a current density of 2 mAh/cm². The excellent stability can be attributed to several factors: i) the high strength of the hydrogel electrolyte can inhibit the formation of Zn dendrites;[8] ii) the abundant hydroxyl and carboxyl functional groups present on the polysaccharide molecular chains can bind with Zn^{2+}, accelerating the deposition kinetics of Zn^{2+} and thereby promoting uniform zinc deposition;[7, 9] iii) the strong hydration of lithium ions contributes to disrupting the directional arrangement of hydrogen bonds in water molecules, decreasing the amount of water molecules coordinated with Zn^{2+} and thus inhibiting side reactions at the zinc electrode.[10] These factors contribute to the rapid transport, uniform distribution of Zn^{2+}, and inhibition of Zn dendrite formation.

Based on above results, the MnO_2 || Zn soft package battery with a sandwich structure, was assembled using MnO_2 as the cathode, zinc foil as the anode, and the PVA/CMC/CCNF-4M hydrogel as the flexible electrolyte (Fig. S9e). According to Fig. S9g, the cyclic voltammetry curves (CV) demonstrate two distinct oxidation peaks and reduction peaks, accompanied by minimal voltage polarization, indicating excellent reversibility of the battery. The similar trends of the curves at different rates suggest rapid charge transfer kinetics. With increasing scan rates, the positive shift of the oxidation peaks and the negative shift of the reduction peaks result from the limited ion diffusion.[11] The EIS spectra show that the battery possesses low charge transfer resistance and diffusion resistance, further confirming its rapid charge transfer kinetics (Fig. S9h).[12] Interestingly, the soft package battery can keep a stable output voltage of 1.4 V (Fig. S9f) and can reliably light up the LED bulb (Fig. S9d) without recharging. More encouragingly, the soft package battery underwent 500 charge-discharge cycles at a current density of 1 A/g, demonstrating superior stability (Fig. S9i). The uniform

deposition of zinc after 500 cycles further confirmed this stability (Fig. S9j). All results indicate that the hydrogel shows significant potential in flexible zinc-ion battery applications.

References

1. G. Fang, J. Zhou, A. Pan and S. Liang, *ACS Energy Letters*, 2018, **3**, 2480-2501.
2. B. Tang, L. Shan, S. Liang and J. Zhou, *Energy & Environmental Science*, 2019, **12**, 3288-3304.
3. Q. Zhang, J. Luan, Y. Tang, X. Ji and H. Wang, *Angewandte Chemie International Edition*, 2020, **59**, 13180-13191.
4. R. Zhu, H. Yang, W. Cui, L. Fadillah, T. Huang, Z. Xiong, C. Tang, D. Kowalski, S. Kitano, C. Zhu, D. R. King, T. Kurokawa, Y. Aoki and H. Habazaki, *Journal of Materials Chemistry A*, 2022, **10**, 3122-3133.
5. Z. Hong, Z. Ahmad and V. Viswanathan, *ACS Energy Letters*, 2020, **5**, 2466-2474.
6. J.-L. Yang, T. Xiao, T. Xiao, J. Li, Z. Yu, K. Liu, P. Yang and H. J. Fan, *Advanced Materials*, 2024, **36**, 2313610.
7. W. Tu, S. Liang, L. Song, X. Wang, G. Ji and J. Xu, *Advanced Functional Materials*, 2024, **24**, 2316137.
8. G. Weng, X. Yang, Z. Wang, Y. Xu and R. Liu, *Small*, 2023, **19**, 2303949.
9. S. Huang, L. Hou, T. Li, Y. Jiao and P. Wu, *Advanced Materials*, 2022, **34**, 2110140.
10. Q. Liu, X. Ou, Y. Niu, L. Li, D. Xing, Y. Zhou and F. Yan, *Angewandte Chemie International Edition*, 2024, **63**, e202317944.
11. Y. Li, R. Miao, Y. Yang, L. Han and Q. Han, *Soft Matter*, 2023, **19**, 8022-8032.
12. G. Cao, L. Zhao, X. Ji, Y. Peng, M. Yu, X. Wang, X. Li and F. Ran, *Small*, 2023, **19**, 2207610.